Growth, structural, optical, thermal, hardness and dielectric studies of rare earth Yttrium doped Tris Thiourea Zinc(II) Sulphate single crystals

K. KANAGASABAPATHY[*], S. VETRIVEL[a], R. RAJASEKARAN[b]
PG & Research Department of Physics, A.A. Government Arts College, Villupuram-605 602, India
[a]PG & Research Department of Physics, Government Arts College, Tiruvannamalai-606 603, India
[b]Thiru. Kolanjiappar Government Arts College, Vriddachalam-606 001, India

Tris thiourea Zinc(II)sulphate (ZTS) and rare earth Yttrium(III)Nitrate doped Tris thiourea Zinc(II)sulphate compounds were synthesized from aqueous solution and single crystals were grown from aqueous solution by slow evaporation technique. The unit cell parameters of the grown crystals were evaluated by single crystal X-ray diffraction analysis. Powder X-Ray diffraction patterns were recorded and indexed for the structural confirmation. The functional groups present in the crystals were analyzed, using the Fourier transform infrared (FTIR) spectral analysis. EDX analysis revealed the incorporation of the Yttrium ions (Y^{3+}) entered into ZTS crystals. UV-Visible transmission spectrum has been recorded to determine the cut-off wavelength of grown crystals for nonlinear applications. TG–DTA studies show thermal stability of the grown crystals. The microhardness studies on the grown crystals revealed that the hardness increases with applied load for all the grown crystals. From the value of work hardening coefficients, it was found that ZTS and Yttrium(III)Nitrate doped ZTS crystals belong to the category of soft materials. The crystal perfection and quality have been identified by etching studies. The dielectric measurement exhibits the dielectric constant and dielectric loss of the grown crystals decrease with increase in frequency. The nonlinear optical properties of pure and Yttrium(III)Nitrate doped ZTS crystals were confirmed by Kurtz-Perry powder method using Nd:YAG laser source.

1. Introduction

In the last few decades, Research in non-linear optical materials have been of great interest due to their potential applications including second-harmonic generation (SHG), frequency mixing, electro-optic modulation, etc. Efforts have been taken to synthesize new materials for variety of nonlinear optical (NLO) applications such as optical signal processing, parametric amplification, optical phase conjugation, etc. Nonlinear optical (NLO) properties have been the subject of numerous investigations by both theoretical and experimental aspects [1,2]. The semi-organic NLO materials have been attracting much attention due to high nonlinearity, chemical flexibility, high mechanical and thermal stability and good transmittance [3]. Tris Thiourea Zinc(II) Sulphate (ZTS) is a novel metal-organic NLO material for second harmonic generation from metal complexes of thiourea. It crystallizes in orthorhombic system with non-centro symmetric space group $Pca2_1$ (point group mm2 and Z=4) [4–6]. Recently, frequency up conversion of infrared light to visible light has been extensively investigated in trivalent rare-earth (RE)-ion-doped materials for a wide range of applications, such as, three-dimension volumetric

display, all-solid-state compact laser devices operating in the blue-green region, optical data storage, infrared quantum counter detectors and fluorescent labels [7,8]. Among trivalent RE-ions, Pr^{3+}, Nd^{3+}, $Er^{3+,}$ $Tm^{3+,}$ and Ho^{3+} ions have been investigated most widely in the last two decades [9]. Recently, rare earth doped crystals and glasses have been extensively investigated owing to their potential applications as fiber amplifier, visible laser, optical data storage, sensors, optical communication and displays [10–12]. Effect of Ce^{3+} doping on the well known NLO crystals of KHP and ZTS has been investigated. Cerium (Ce^{3+}) dopant could occupy the substitutional site without producing any stress in the crystal lattices of ZTS leading to improvement in the crystalline perfection followed by a significant enhancement in the SHG efficiency [13].

Recently, we have investigated the effect of doping rare earth ions Nd^{3+} [14], Ce^{3+} [15] on ZTS crystals. A systematic investigation on the dopant effect of trivalent Rare Earth Yttrium(Y^{3+}) ions into the growth medium of ZTS single crystals have not been reported until recently. In the present investigation, the effect of Y^{3+} doping on ZTS crystals have been studied using XRD, FT-IR, UV–vis, thermal, dielectric, microhardness and Kurtz powder SHG measurements.

2. Experimental details

2.1. Synthesis and crystal growth

ZTS compound was synthesized from stoichiometric incorporation of analar grade thiourea (99% Merck) and zinc sulphate heptahydrate (99% Merck). The thiourea and zinc sulphate heptahydrate were taken in the ratio 3:1 and the calculated amount of thiourea and   zinc sulphate heptahydrate were dissolved in deionised water of resistivity 18.2 MΩcm (Millipore). The ZTS compound was prepared according to the following reaction,

$$3(CH_4N_2S) + ZnSO_4.7H_2O \rightarrow Zn[(CH_4N_2S)]_3SO_4 + 7H_2O$$
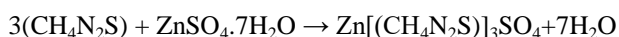
The synthesized salt was further purified by repeated recrystallization process. A saturated aqueous solution was prepared and kept at room temperature for slow evaporation. Good quality single crystal with perfect external morphology and size of 11 mm × 10 mm × 6 mm was harvested within 20 days. For the growth of Yttrium ions doped ZTS crystals, 1mol% of Yttrium(III) Nitrate [$Y(NO_3)_3 6H_2O$] was added to the solution of ZTS. Single crystals of size 12 mm × 8 mm × 6 mm with perfect external morphology and good transparency were grown in 35–40 days. Figs. 1a &1b and Figs. 2a & 2b show the as-grown crystals and morphology of pure and doped ZTS crystals respectively.
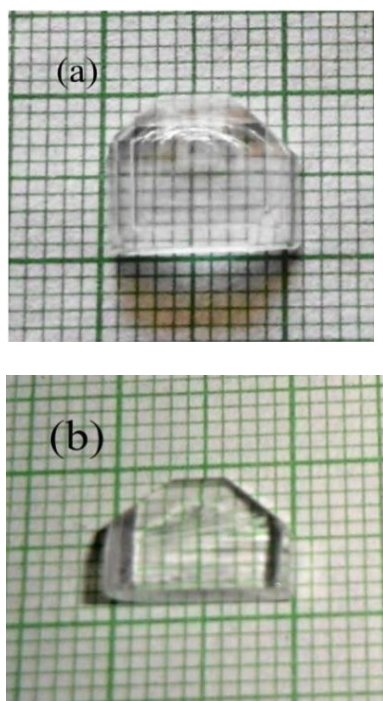
Fig. 1. Photographs of (a) ZTS (b) Y^{3+} doped ZTS crystals

(a)

(b)
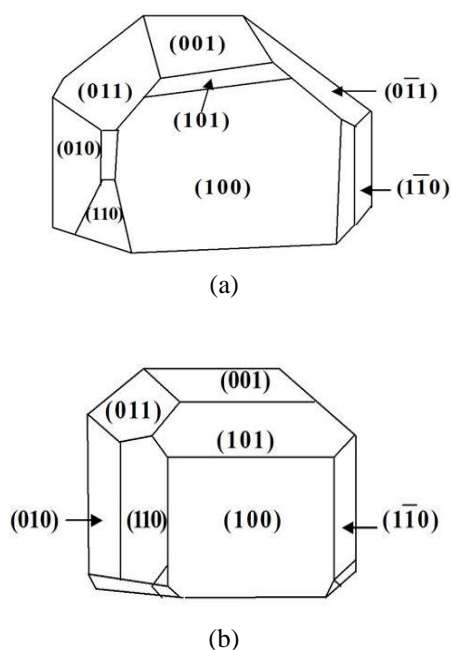
Fig. 2. Morphology of (a) ZTS and
(b) Y^{3+} doped ZTS crystals

2.2. Characterization techniques

The grown crystals were subjected to single crystal X-ray diffraction (XRD) studies using a Kappa ApexII Nonius CAD4 diffractometer with MoK_α radiation (λ = 0.71073 Å). Powder XRD pattern of the grown crystal was recorded between 10°and 80° in steps of 2° employing CuK_α radiation (λ=1.5406Å) using Bruker powder X-ray Diffractometer.   FTIR spectra of pure and Yttrium(III) Nitrate doped ZTS was recorded by Alpha Bruker spectrometer in the wave length range 400-4000 cm^{-1}. Energy dispersive X-ray spectroscopy (EDX), a chemical microanalysis technique was performed on the grown crystals in conjunction with SEM using a JEOL JSM 5610 LV Scanning Electron Microscope with an accelerating voltage of 20 kV. Optical transmission of the crystal was recorded using VARIAN 5000 UV-visible spectrophoto meter in the wavelength region 200–900 nm. In order to estimate the thermal behaviour, simultaneous thermo gravimetric analysis (TGA) and differential thermal analyses (DTA) of pure and Yttrium(III)Nitrate doped ZTS were carried out by TA Instruments Q 600 SDT Thermal Analyzer in the temperature range: RT to 800 °C (SiC furnace). The microhardness studies were carried out on the grown crystals using Vicker's Microhardness tester. The dielectric measurements were carried out using a HIOKI HITESTER model 3532–50 LCR meter in the frequency range 1kHz–3 MHz at different temperatures. Nonlinear optical property of ZTS and Y^{3+}doped ZTS compound was confirmed by shining Nd:YAG laser source of wavelength 1064 nm.

3. Results and discussion

3.1. Structural analyses

3.1.1. Single crystal X-ray diffraction analysis

X-ray diffraction analysis of pure and 1mol% Y^{3+} doped ZTS crystals were carried out and their respective lattice parameter values are presented in Table 1.

Table 1. Lattice parameter values of the grown crystals

Crystal	a(Å)	b(Å)	c (Å)	V(Å³)	α = β = γ
Tris thiourea Zinc(II) Sulphate	7.77	11.14	15.50	1341.65	90°
Y^{3+} doped ZTS	7.82	11.18	15.51	1356.00	90°

The grown crystals belong to orthorhombic system with space group Pca2$_1$ and point group mm2. The increase in volume may be due to the addition of rare earth Y^{3+} ions in ZTS. These values are in close agreement with the corresponding JCPDS (76-0778) values for pure ZTS with very nominal changes due to doping [16]. From single crystal X-ray diffraction analysis, it is confirmed that the addition of Rare Earth ions alters the lattice parameter values without affecting the basic structure of crystal [17,18].

3.1.2. Powder X-ray diffraction analysis

The Bragg's reflections in the powder XRD patterns (Fig.3) were indexed for pure and Y^{3+} doped ZTS crystals. The diffraction curve of ZTS shows a set of prominent peaks corresponding to (002), (111), (200), (201), (210), (211), (311), (221), (321), (123), (410), (224), (431) and (428) planes. For the 1mol% of Yttrium(III) Nitrate doped ZTS, the peak intensities of reflections values (401) and (431) have been increased with doping, the peak intensities of reflections values (002), (111),(200) and (123) have been reduced with doping and peaks (201), (210), (410), (323), (227) and (428) have been diminished with doping and few new peaks (220), (315), (620) and (521) also appeared due to doping. Comparing the powder XRD pattern, there is a small shift in the doped XRD pattern of ZTS. This confirms the incorporation of trivalent Yttrium ions in the ZTS crystal lattice. The observed values are in good agreement with the reported values [16]. The slight change in unit cell volume may be due to change in pH of the solution due to the addition of dopant [19].
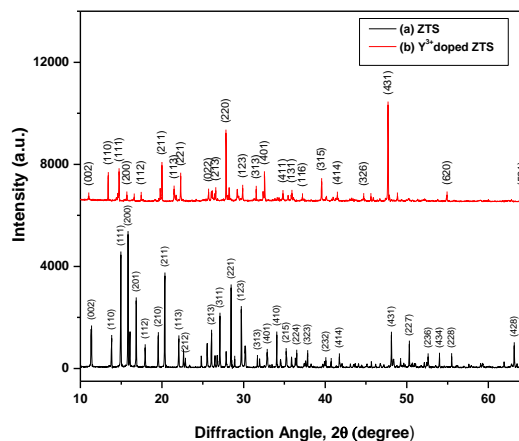
Fig. 3. Powder XRD patterns of (a) ZTS and (b) Y^{3+} doped ZTS crystals

3.2. FTIR studies

FTIR spectra of pure and 1mol% Y^{3+} doped ZTS is shown in Fig. 4. From the spectral analysis, the thiourea crystal exhibits the bands in the region   400 – 750 cm^{-1}, 1050 – 1150 cm^{-1} and 1300 – 1650 cm^{-1}. These bands arise due to the strong coupling between C=S, C-N and δ(NH$_2$) vibrations respectively. The very strong vibrational lines observed at 740 and 1417 cm^{-1} in FTIR spectrum are due to the CS symmetric and asymmetric stretching vibrational modes respectively. The strong peaks at 1089 and 1472 cm^{-1} have been assigned to CN symmetric and asymmetric stretching vibrational modes. The intense peak at 1627 cm^{-1} is due to NH$_2$ asymmetric bending vibrations [20]. The high wave number region(3100–3400cm^{-1})   arises due to NH stretching vibrations [21]. These vibrational assignments are taken into account in assigning the FTIR bands in pure and rare earth Yttrium ions doped ZTS crystals.

The CS stretching (1417 cm^{-1}) vibration of thiourea is shifted to lower values of pure (1400 cm^{-1}) and Y^{3+} (1400 cm^{-1}) doped ZTS. This clearly indicates the coordination of sulphur with metals. The CN stretching (1089 cm^{-1} and 1472 cm^{-1}) vibrations of thiourea are shifted to higher values of pure (1124 cm^{-1} and 1504cm^{-1}) and Y^{3+} (1128cm^{-1} and 1512 cm^{-1}) doped ZTS. This clearly establishes the delocalization of nitrogen lone pair electron over carbon sulphur double bond, which is an essential property for NLO materials. The absorption bands observed at 1627 cm^{-1} (pure ZTS) and 1630 cm^{-1}(Y^{3+} doped ZTS) are assigned to the NH$_2$ asymmetric bending vibrations. The broad envelope positioned between 2710–3400 cm^{-1} corresponds to the symmetric and asymmetric stretching modes of NH$_2$ grouping of ZTS crystals. The non-shifting of NH vibration bands indicates that the metal is not coordinated through nitrogen, but through sulphur [17, 20]. Although the spectrum of RE^{3+} ions doped ZTS provides similar features as that of pure ZTS, the shift observed for all the peaks suggesting the wide range of interactions of the functional groups. It is also observed that the broadening or narrowing of some absorption peaks in the doped ZTS due to the incorporation of trivalent RE Yttrium ions in

the lattice of ZTS. Hence, FTIR spectral studies indirectly establish the presence of Y^{3+}ions in the lattice of ZTS crystal.
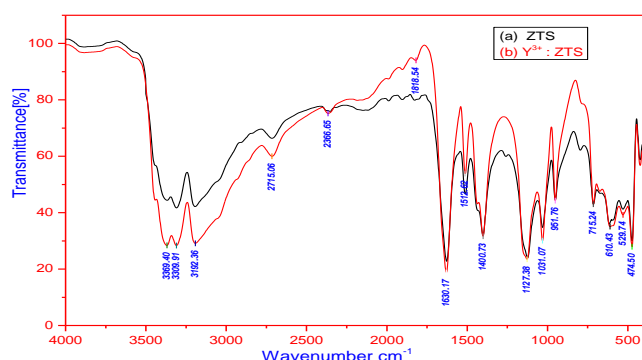
Fig. 4. FTIR spectrum of pure and Y^{3+} doped ZTS crystals

3.3. EDX analysis

The presence of Yttrium in the doped specimen was confirmed by EDX analysis and the concentration of the incorporated Y^{3+} into the ZTS crystalline matrix can be clearly seen in Fig. 5. The surface analysis at different sites reveals that the incorporation of Y was found to be non-uniform over the whole crystal surface. The amount of Y^{3+} incorporation into ZTS lattice is given in Table 2.
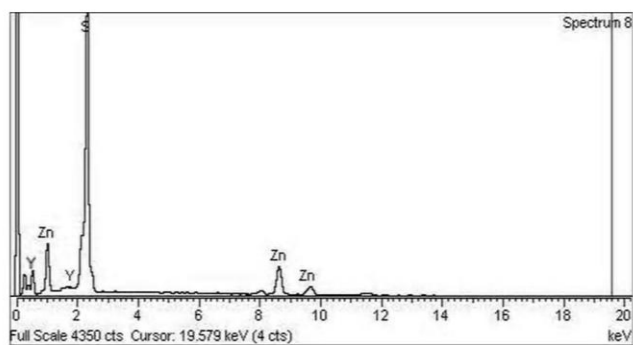
Fig. 5. EDX spectrum of Y^{3+} doped ZTS single crystal

Table 2. EDX data for Yttrium doped ZTS crystal

Element	Weight %	Atomic %
S	52.51	73.24
Zn	46.44	26.72
Y	1.05	0.04

3.4. UV–visible spectral analysis

Good optical transmittance and lower UV cut-off wavelengths are very important properties for NLO

crystals. Optical transmittance spectra pure ZTS and 1mol% Yttrium doped ZTS are shown in Fig. 6. It is clear from the spectra that the percentage of optical transmission for pure ZTS crystal is 73% at 800 nm and it increases with Y doping (79%). Near UV region, absorption arises from electronic transition associated within the thiourea units of ZTS. The orbital P electron delocalization in thiourea arises from the mesomeric effect. This P electron dislocation is responsible for its nonlinear optical response and absorption in near UV region [22]. This is one of the most desirable properties of the grown crystals for the device fabrication. From UV–visible spectral analysis, it is noted that there is a maximum transmittance in the entire visible region, which enables it to be a potential candidate for optoelectronic applications. [23].
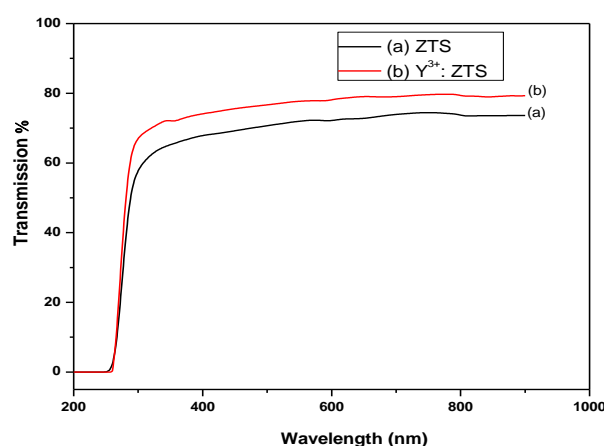
Fig. 6. UV-Visible transmission spectra of (a) ZTS and (b) Y^{3+}: ZTS crystals

The band gap energy (E_g) can be calculated directly from the UV-cutoff wavelength by using the relation, $E_g = hc / \lambda_{(cut)}$ eV where E_g is the band gap energy, $h = 6.626 \times 10^{-34}$ J/s, $c = 3 \times 10^{8}$ m/s , $\lambda_{(cut)}$ is the UV cut-off wavelength. The band gap energies were found to be 4.647 eV for pure ZTS and 4.613 eV for Y^{3+} doped ZTS [24]. The pure and Y^{3+} doped ZTS crystals were identified to be wide band gap material.

3.5. Thermal analysis

The thermal analysis was carried out in the temperature range 25°-600°C at a heating rate of 25°C /min. DTA curve for ZTS (Fig. 7a) shows a sharp endothermic transition at 238.4ºC. Further endothermic peaks are observed at 301.8ºC and 361.6ºC. DTA curve of Y^{3+} doped ZTS (Fig. 7b) shows three endothermic transitions with the first one at 238.13ºC, the second at 300.7ºC and the third at 362.32ºC. The first endothermic peak coincides with the decomposition of the crystal (238.13ºC). The melting point of doped ZTS is observed at 238.4ºC. When Yttrium doped with ZTS, the decomposition of ZTS is decreasing slightly.

From the TG curve, the weight loss in the temperature range 218ºC–380ºC is due to the liberation of volatile

substances like sulphur oxide in the compound [20]. It is observed that maximum weight loss occurred in the temperature range 225–380ºC compared with subsequent stages. A total weight loss of about 69.8% occurred only at 600 °C for doped ZTS crystal. This shows the thermal stability of the crystal. It is concluded that the thermal stability of ZTS slightly decreasing with trivalent Yttrium doping. The absence of water in molecular structure is confirmed by the absence of weight loss around 100 °C. There is no decomposition upto melting point, this insures thermal stability of   material for possible application in lasers. Fig. 7 shows TG – DTA curves of (a) ZTS and   (b) Y^{3+} doped ZTS crystals.
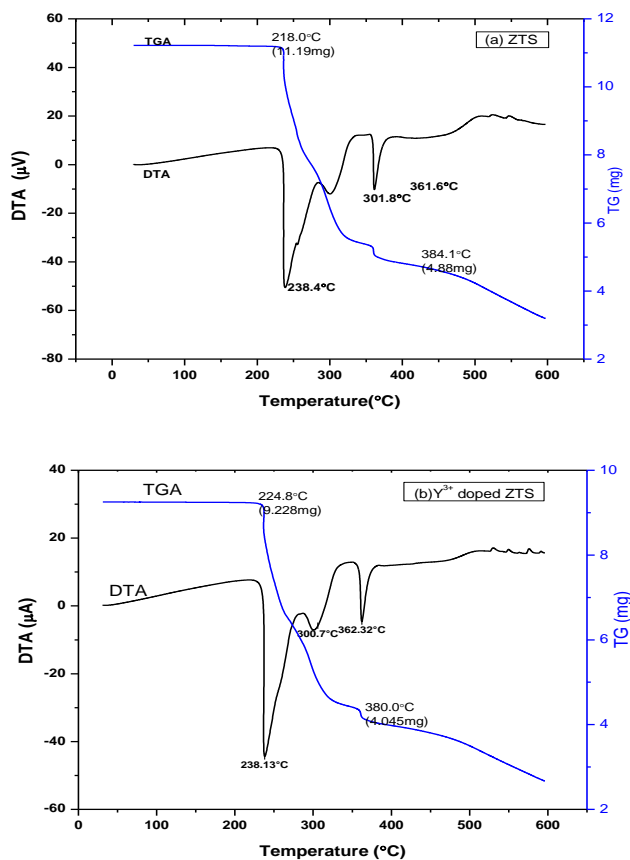
Fig. 7. TG–DTA curves of (a) ZTS and (b) Y : ZTS crystals

3.6. Microhardness studies

Indentations were made on (100) plane of pure and rare earth doped ZTS crystals using a Vicker's indenter for various loads. The hardness number of the grown crystals have been calculated using the relation $H_v = 1.8544 \, (P/d^2)$ kg/mm^2 where H_v is the Vicker's hardness number, P is the applied load in kg and d is the average diagonal length of the indented impression in mm. It has been observed that the hardness value increases with applied load upto P=50 g due to work hardening of the surface layer in ZTS crystal. Above 50 g, cracks were formed. In Yttrium doped ZTS crystals, the hardness value is slightly lower than ZTS due the dopant effect and above 40 g, cracks were formed

due to the release of internal stress generated locally by indentation. A plot drawn between Hardness value H_v and load P is shown in the Fig. 8. The plot of log P against log d is a straight line (Fig. 9) which is in good agreement with Meyer's law P = a d^n. From the slope of the graph, the work hardening coefficient (n) for ZTS crystal is found to be 3.63 which is in good agreement with the reported value [25]. The obtained values of work hardening coefficient for 1mol% of Yttrium doped ZTS crystal was estimated as 3.23. Onitsch et al. [26] reported the values of n for which if $1 \leq n \leq 1.6$ for hard materials and $n \geq 1.6$ for soft materials. Since the obtained values of 'n' for the grown crystals are more than 1.6, the grown crystals of this work belong to the soft category materials. In both the grown crystals, the hardness increases with the increase in applied load (P) and hence refers to Reverse Indentation Size Effect (RISE). The increase of hardness number with load will be useful for nonlinear optical applications.
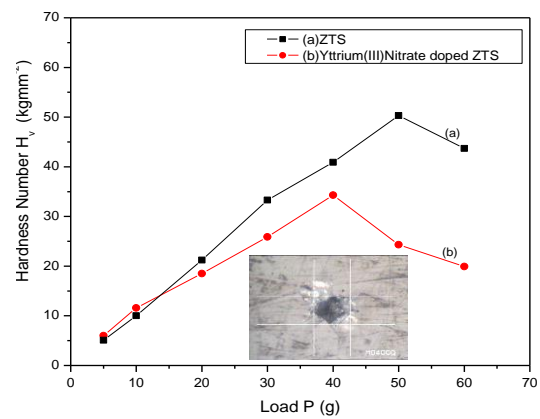
Fig. 8. Plot of Hardness vs. applied load
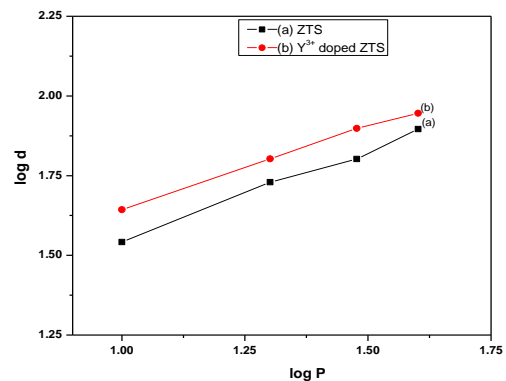
Fig. 9. Plot of log P versus log d

3.7. Etching analysis

The chemical etching technique is the simplest characterization technique that can be best employed to study the defect in structure of a single crystal. However, the success of this technique lies in the efficiency of the chemical etchant to sense the dislocation site selectively. Subsequently, etch pits are formed at the dislocation centers on those faces at which the additives are bound,

which is able to develop some of the features such as growth hillocks, etch spirals, triangular and rectangular etch pits, etc. on the surface. Device fabrication and technical applications require crystal of high quality or at least of known and well-defined defects structure [27]. Etching was carried out using deionised water as an etchant at room temperature. Once the damaged surface layer was removed by means of etching, a fresh surface appeared, which in turn gave clear etch pits. The etched surface was soaked with a good quality (wrinkle free) filter paper and the samples were immediately examined and their microstructure was analyzed using an optical microscope (Reichert Polyvar2 MET– Leica make) in the reflection mode. Fig. 10(a) represents the well defined pyramidal shape of etch pits observed in the grown Yttrium doped ZTS crystal and the calculated etch pit density (EPD) was 16.8×10^2 cm^{-2}. The pyramidal shape of etch pits was damaged while increasing the etching time from 10 to 30 s. Chemical etching studies were carried out on the conventional methods on (1 0 0), (0 0 1) plane of ZTS crystals and the EPD was 10^2 and 10^3 cm^{-2}. Fig. 10(b) represents the etch pits observed for the grown Yttrium doped ZTS on (1 0 0) direction and the EPD was 8.7×10^2 cm^{-2}. The reduced EPD in KDP and TGS crystals have been already reported [28, 29].
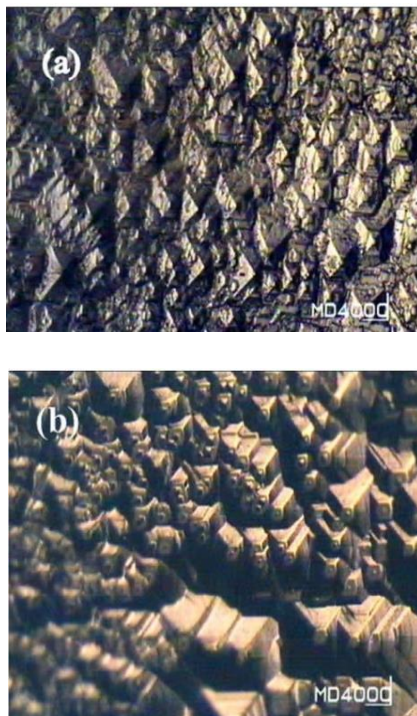
Fig. 10. Etch patterns produced on the (100) plane of Y^{3+} doped ZTS crystal with etching time (a) 10 s   (b) 30 s

3.8. Dielectric studies

The dielectric constant is one of the basic electrical properties of solids. The variation of dielectric constant and dielectric loss with log frequency at different temperatures of pure ZTS and Y : ZTS crystals are shown in Fig. 11 and 12. The dielectric constant decreases very rapidly at low frequencies and slowly at higher frequencies. From the plots, it is observed that the dielectric constant decreases with increasing frequency and attain saturation at higher frequencies. Dielectric studies furnish a great deal of information regarding the dielectric constant that arises from the contribution of different polarizations, namely electronic, ionic, atomic, space charge, etc., developed in the material subjected to the electric field variations. The large dielectric constant at low frequency for the crystals in the present study is due to the presence of space charge polarization arising at the grain boundary interfaces [30].
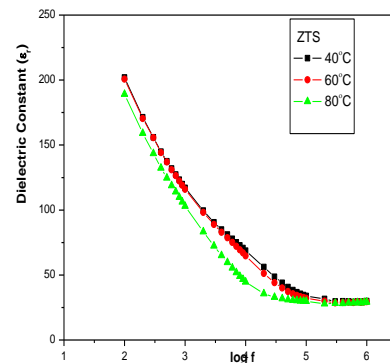
Fig. 11(a). Variation of dielectric constant vs. log frequency of ZTS
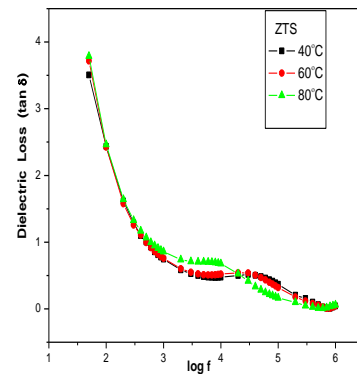
Fig. 11(b). Variation of dielectric loss vs. log frequency of ZTS
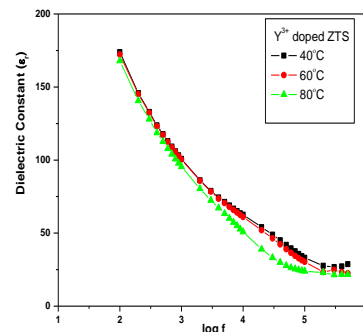
Fig. 12(a). Variation of dielectric constant vs. log frequency of Y^{3+} doped ZTS
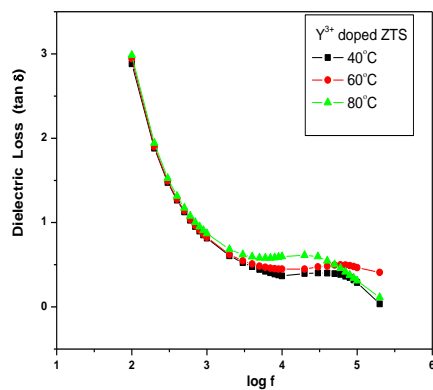
*Fig. 12(b). Variation of dielectric loss vs.
log frequency of Y^{3+} doped ZTS*

The low values of dielectric constant at higher frequencies reveal the good optical quality of the grown crystals with less defects, which is the desirable property of the materials to be used for various optical and communication devices [31]. The dielectric constant measured at different temperatures almost remains the same at higher frequencies. It indicates that the temperature variation has no influence on the dielectric property of the material. The electronic exchange of a number of ions in the crystals gives local displacement of electrons in the direction of the applied field, which in turn gives rise to polarization.

The dielectric loss is also studied as a function of frequency at 40°C, 60°C, 80°C, for both pure and Y^{3+} doped ZTS crystals, as shown in Figs. 11(b), 12(b). These curves suggest that the dielectric loss strongly depends on the frequency of the applied field similar to what commonly happens with the dielectric constant in the ionic system [32, 33]. The dielectric loss decreases with increase in frequency at almost all temperatures. At higher frequencies, the measure of dielectric loss is relatively low since the electric wave frequency is not equal to that of natural frequency of the bounded charge, and hence the radiation is very weak. The measure of low dielectric loss at various frequencies is also due to dipole rotations. At high frequencies orientation polarization ceases and hence the energy need not be spent to rotate dipoles. The characteristic studies of dielectric constant and dielectric loss with higher frequencies of pure and Y^{3+} doped ZTS crystals suggest that the samples possess enhanced optical quality with lesser defects and this parameter is of vital importance for nonlinear optical applications [34].

3.9. NLO property studies

The qualitative measurement of the second harmonic generation (SHG) efficiency was determined using powder technique developed by Kurtz and Perry [35]. For the SHG efficiency measurements, the output of a Q-switched, mode-locked Nd:YAG laser was used to generate about 2·8 mJ/pulse at 1064 nm fundamental radiation. A single shot mode of 8 ns laser pulse at a repetition rate of 10 Hz

with a spot radius of 1 mm was used. This experimental set up used a mirror and 50/50 beam splitter to generate a beam with pulse energies of about 2·8 mJ. The input laser beam was allowed to pass through an IR reflector and then directed on the micro-crystalline powdered sample packed in a capillary tube of diameter 0·154 mm. The photodiode detector and oscilloscope arrangement measured the light emitted by the sample. For the Nd:YAG laser, the fundamental beam of 1064 nm generates second harmonic signal of 532 nm(green light). The output pulses measured for ZTS and Y^{3+} doped ZTS are given Table 3. The effect of various rare earth dopant on the SHG efficiency of the ZTS crystal has also been listed in the Table 3.

*Table 3. SHG output signal voltages of pure and rare
earth doped ZTS crystals*

Samples	$I_{2\omega}$ (mV)	SHG efficiency	Reference
ZTS	18	1.00	[14,15]
Y^{3+} doped ZTS	21	1.17	Present study
Ce^{3+} doped ZTS	17	0.94	[15]
Nd^{3+} doped ZTS	31	1.72	[14]

The enhancement of SHG efficiency for Y^{3+} doped ZTS is due to the optically active rare earth Yttrium which may get added into the structure and increases its non-centro symmetry and hence increasing its SHG efficiency of ZTS crystal.

4. Conclusion

Optical quality single crystals of ZTS and Yttrium (III) Nitrate doped ZTS crystals were grown from solution by slow evaporation technique. Single crystal X-ray diffraction confirms that there is no change in basic structure of ZTS. From the powder XRD pattern, the prominent well-resolved peaks at specific 2θ angle reveal the high crystalline nature of the crystal. FTIR study confirms the presence of all functional groups in the grown crystals. SEM-EDX analysis confirms the presence of Y in the doped specimen. UV-Visible study shows that the grown crystals have wide range of transparency in UV and entire visible region and cut-off wavelength was found to be around 268 nm. TG–DTA analyses show that the grown crystal has very good thermal stability upto 238°C. Microhardness studies showed that Hardness number (H_v) increases with the increase of loads. The work hardening co-efficient of the grown crystals were calculated. The crystalline perfection was confirmed by etching studies. The variation of dielectric constant as function of frequency suggests that the dielectric constant is relatively higher at low frequency region and lower in the higher frequency region. The SHG efficiency enhances (1.17 times) for Y^{3+} doped ZTS crystal as compared with pure ZTS crystal. Thus, the 1mol% Y^{3+} doped ZTS crystal will

play vital role in the field of optoelectronics and laser technology.

References

[1] R.W. Boyd, Academic Press, San Diego, 1992.

[2] D. S. Chemla, J. Zyss, **I** and **II**, Academic Press, New York, 1987.

[3] M. Jiang, Q. Fang, Adv. Mater. **11**, 1147 (1999).

[4] P. M. Ushasree, R. Jayavel, C. Subramanian, P. Ramasamy, J. Cryst. Growth **197**, 216 (1999).

[5] H. O. Marcy, L. F. Warren, M. S. Webb, C. A. Ebbers, S. P. Velsko, G. C. Kennedy, G. C. Catella, Appl. Opt. **31**, 5051 (1992).

[6] V. Venkataramanan, G. Dhanaraj, W. K. Wadhavan, J. N. Sherwood, H. L. Bhat, J. Cryst. Growth **154**, 92 (1995).

[7] P. Lecoq, IEEE Trans. Nucl. Sci. **40**, 409 (1993).

[8] W. Dianyuan, G. Yanyan, W. Xinghua, Z. Yuxia, J. Rare Earth **26**, 880 (2008).

[9] D. Y. Wang, J. L. Luo, J. M. Yu, J. Q. Liu, Q. K. Wang, Y. Y. Guo, M. Yin, W. P. Zhang, S. D. Xia, J. Alloys Compd. **399**, 57 (2005).

[10] C. W. E. van Eijk, J. Andriessen, P. Dorenbos, R. Visser, Nucl. Instr. Methods. Phys. Res. Sec. A **348**, 546 (1994).

[11] P. H. Holloway, T. A. Trottier, S. L. Jones, J. S. Sebastian, W. J. Thomes, J. Vac. Sci. Tech. B **17**, 758 (1999).

[12] M. Iwasaki, J. Kuraki, S. Ito, J. Sol-Gel Sci. Tech. **13**, 587 (1998).

[13] L. Kasthuri, G. Bhagavannarayana, S. Parthiban, G. Ramasamy, K. Muthu, S. Meenakshisundaram, Cryst. Engg. Commn. **12**, 493 (2010).

[14] K. Kanagasabapathy, R. Rajasekaran, Adv. Mater. Res. **584**, 37 (2012).

[15] K. Kanagasabapathy, R. Rajasekaran, Optik **124**, 4240 (2013).

[16] G. D. Andreetti, L. Cavalca, A. Musatti, Acta. Crystallogr. **B24**, 683 (1968).

[17] P. M. Ushasree, R. Jayavel, P. Ramasamy, Mater. Chem. Phys. **61**, 270 (1999).

[18] M. Katsurayama, Y. Anzai, A. Sugiyama, M. Koike, Y. Kato, J. Cryst. Growth **229**, 193 (2001).

[19] G. Arunmozhi, M. de Gomes, S. Ganesamoorthy, Cryst. Res. Technol. **39**, 408 (2004).

[20] J. Ramajothi, S. Dhanuskodi, K. Nagarajan, Cryst. Res. Technol. **39**, 414 (2004).

[21] S. P. Meenakshisundaram, S. Pathiban, N. Sarathi, R. Kalavathy, G. Bhagavanarayana, J. Cryst. Growth **293**, 376 (2006).

[22] R. Rajasekaran, R. Mohan Kumar, R. Jayavel, P. Ramasamy, J. Cryst. Growth **252**, 317 (2003).

[23] R. BairavaGanesh, V. Kannan, R. Sathyalakshmi, P. Ramasamy, Mater. Lett. **61**, 706 (2007).

[24] M. Selvapandiyan, J. Arumugam, P. Sundaramoorthi, S. Sudhakar, J. Alloys Compd. **558**, 34 (2013).

[25] S. Dhanuskodi, T. C. Sabari Girisun, J. Cryst. Growth **330**, 43 (2011).

[26] E. M. Onitsch, Mikroskopie, **2**, 131 (1947).

[27] L. Owczarek, K. Sangwal, J. Cryst. Growth **99**, 827 (1990).

[28] S. Balamurugan, P. Ramasamy, Mater. Chem. Phys. **112**, 1 (2008).

[29] M. Senthil Pandian, N. Balamurugan, V. Ganesh, P. V. Raja Shekar, K. Kishan Rao, P. Ramasamy, Mater. Lett. **62** 3830 (2008).

[30] S. Ishwar Bhat, P. Mohan Rao, A. P. Ganesh Bhat, D. K. Avasthi, Surf. Coat. Technol. **158**, 725 (2002).

[31] C. Balarew, R. Duhlew, J. Solid State Chem. **55**, 1 (1984).

[32] K. V. Rao, A. Smakula, J. Appl. Phys. **37**, 319 (1966).

[33] K. V. Rao, A. Smakula, J**.** Appl**.** Phys. **36**, 2031 (1965).

[34] G. Anandha Babu, G. Bhagavanarayana, P. Ramasamy, J. Cryst. Growth **310**, 2820 (2008).

[35] S. K. Kurtz, T. T. Perry, J. Appl. Phys. **39**, 3798 (1968).

---
[*]Corresponding author: kksaba98@gmail.com